

Stratospheric Ozone Changes Damp the CO₂-Induced Acceleration of the Brewer–Dobson Circulation

LEONHARD HUFNAGL¹,^a ROLAND EICHINGER¹,^{a,c} HELLA GARNY¹,^{a,b} THOMAS BIRNER¹,^b ALEŠ KUCHAR¹,^d
PATRICK JÖCKEL¹,^a AND PHOEBE GRAF¹,^a

^a *Institut für Physik der Atmosphäre, Deutsches Zentrum für Luft- und Raumfahrt (DLR), Oberpfaffenhofen, Germany*

^b *Institut für Meteorologie, Ludwig-Maximilians-Universität, Munich, Germany*

^c *Department of Atmospheric Physics, Faculty of Mathematics and Physics, Charles University, Prague, Czech Republic*

^d *Institut für Meteorologie, Universität Leipzig, Leipzig, Germany*

(Manuscript received 7 July 2022, in final form 11 January 2023)

ABSTRACT: The increase of atmospheric CO₂ concentrations changes the atmospheric temperature distribution, which in turn affects the circulation. A robust circulation response to CO₂ forcing is the strengthening of the stratospheric Brewer–Dobson circulation (BDC), with associated consequences for transport of trace gases such as ozone. Ozone is further affected by the CO₂-induced stratospheric cooling via the temperature dependency of ozone chemistry. These ozone changes in turn influence stratospheric temperatures and thereby modify the CO₂-induced circulation changes. In this study, we perform dedicated model simulations to quantify the modification of the circulation response to CO₂ forcing by stratospheric ozone. Specifically, we compare simulations of the atmosphere with preindustrial and with quadrupled CO₂ climate conditions, in which stratospheric ozone is held fixed or is adapted to the new climate state. The results of the residual circulation and mean age of air show that ozone changes damp the CO₂-induced BDC increase by up to 20%. This damping of the BDC strengthening is linked to an ozone-induced relative enhancement of the meridional temperature gradient in the lower stratosphere in summer, thereby leading to stronger stratospheric easterlies that suppress wave propagation. Additionally, we find a systematic weakening of the polar vortices in winter and spring. In the Southern Hemisphere, ozone reduces the CO₂-induced delay of the final warming date by 50%.


SIGNIFICANCE STATEMENT: A robust circulation response to enhanced CO₂ is the strengthening of the equator-to-pole circulation in the stratosphere, the so-called Brewer–Dobson circulation (BDC), which affects the ozone layer by tracer transport. This in turn alters stratospheric temperatures and thereby modifies the stratospheric circulation. In the present study, we perform model experiments to quantify the ozone-induced circulation changes caused by quadrupled CO₂ concentrations. The results show that ozone changes damp the CO₂-induced BDC strengthening due to radiative effects of the redistributed ozone layer by enhanced CO₂. These ozone modifications lead to strengthened stratospheric easterlies in summer and decelerated westerlies in winter and spring. Moreover, the ozone changes reduce the CO₂-induced delay of the polar vortex break down date in the Southern Hemisphere.


KEYWORDS: Atmospheric circulation; Climate change; Climate prediction; Ozone; Climate models

1. Introduction

Climate change is an ongoing phenomenon and a result of increasing atmospheric greenhouse gas (GHG) concentrations, which warm the troposphere and cool the stratosphere (Stocker et al. 2013). In the upper troposphere and lower stratosphere region (UTLS), this modifies the zonal wind balance, strengthening the subtropical jets (STJ) and shifting them upward (e.g., Vallis et al. 2015; Chiodo and Polvani

2019; Pisoft et al. 2021). Additionally, it is well established that larger atmospheric concentrations of GHGs strengthen the stratospheric meridional overturning circulation [the Brewer–Dobson circulation (BDC), see Brewer 1949; Dobson 1956], enhancing the transport of trace gases such as ozone from the tropical to the extratropical stratosphere (e.g., Li et al. 2008; McLandress and Shepherd 2009; Garcia and Randel 2008; Eichinger et al. 2020). Moreover, stratospheric cooling leads to a higher net production of ozone (Haigh and Pyle 1982). As a result of these processes, ozone concentrations

 Denotes content that is immediately available upon publication as open access.

 Supplemental information related to this paper is available at the Journals Online website: <https://doi.org/10.1175/JCLI-D-22-0512.s1>.

Corresponding author: Leonhard Hufnagl, leonhard.hufnagl@gmx.net



This article is licensed under a [Creative Commons Attribution 4.0 license](http://creativecommons.org/licenses/by/4.0/) (<http://creativecommons.org/licenses/by/4.0/>).

Publisher's Note: This article was revised on 27 April 2023 to include an updated version of the supplemental file, which contained an error when originally published.

DOI: 10.1175/JCLI-D-22-0512.1

© 2023 American Meteorological Society. For information regarding reuse of this content and general copyright information, consult the [AMS Copyright Policy](https://www.ametsoc.org/PUBSReuseLicenses) (www.ametsoc.org/PUBSReuseLicenses).

decrease in the tropical lower stratosphere and increase in the extratropical and the upper stratosphere.

Ozone is essential for life on Earth. It absorbs high-energetic UV radiation in the stratosphere, but it also acts as an important radiatively active gas (e.g., Thompson et al. 2011). The absorption and emission of shortwave and longwave radiation by ozone thus modifies atmospheric temperatures, especially in the stratosphere. In further consequence, the modifications of the temperature by ozone additionally alter the stratospheric circulation in accordance. However, as this effect is inherent in chemistry–climate model simulations, dedicated model experiments have to be set up in order to disentangle the specific role of CO₂-induced ozone changes for the overall climate response.

A number of recent studies have addressed the question of modulations of the circulation response to CO₂ via stratospheric ozone. For example, Nowack et al. (2018) showed that the ozone changes decrease temperatures in the tropical lower stratosphere and increase temperatures in the extratropical lower stratosphere as a result of radiative effects. The resulting weakened meridional temperature gradient translates into weaker annual mean stratospheric zonal flow. Chiodo and Polvani (2019) asserted that the downward extension of this anomaly to the Southern Hemisphere (SH) troposphere damps the CO₂-induced poleward shift of the eddy-driven jet (EDJ) in their model experiment. Another recent study reported that the CO₂-induced ozone changes weaken the tropical upwelling (DallaSanta et al. 2021). Next to those effects on stratosphere (troposphere) circulation, the CO₂-induced ozone changes also lead to an additional effect of radiative forcing on surface climate, and thus can alter the global mean surface temperature response to CO₂ increases. This modification of the climate sensitivity via stratospheric ozone feedbacks is estimated to be negative, with reductions ranging between 0% and 20% by several studies (Dietmüller et al. 2014; Marsh et al. 2016; Muthers et al. 2014; Nowack et al. 2015; Dacie et al. 2019) and the recent IPCC report (Szopa et al. 2021) assessed that the effects are likely to be closer to the lower bound of those estimates which is 0.064 W m^{−2} K^{−1}.

Overall, these studies mentioned above emphasize the relevance of a realistic ozone representation in climate models, but also motivate further analyses with respect to ozone-induced changes in atmospheric circulations. In particular, the effects of CO₂-induced ozone changes on the BDC have not been investigated in detail so far. A weakening of tropical upwelling as found by DallaSanta et al. (2021) can have consequences for tracer transport in the entire stratosphere, thereby affecting radiation in various manners, which yet has to be quantified in order to assess its contribution to climate change.

In this study, we aim to investigate the effects of ozone-circulation two-way coupling for the circulation response to CO₂ for equilibrated climate states. For that reason, we performed an experiment with the ECHAM/MESSy Atmospheric Chemistry (EMAC; Jöckel et al. 2005, 2010, 2016) model, in which preindustrial and quadrupled CO₂ climate conditions are used. In the simulations with quadrupled CO₂ climate conditions, ozone is once held fixed and is once adapted to the new climate state. The model setup for the preindustrial and the 4xCO₂ simulations that are used here and the data analysis methods are described in section 2. In section 3,

several BDC diagnostics are evaluated to assess how much they are affected by the ozone changes in the 4xCO₂ model simulation. The analysis of the thermal and dynamical impacts that can explain the BDC changes are discussed in section 4, and further effects on the polar vortices in section 5. The results are then summarized and discussed in section 6 before the paper ends with the conclusions in section 7.

2. Data and methods

a. Model and setup

For this study, simulations were conducted with the European Center Hamburg Model/Modular Earth Submodel System (ECHAM/MESSy) Atmospheric Chemistry (EMAC; Jöckel et al. 2005, 2010, 2016) model version 2.54.0.3. The simulations were performed in atmosphere-only model with a T42L47MA resolution, i.e., with a horizontal resolution of $\sim 2.8^\circ \times 2.8^\circ$ in latitude and longitude of the corresponding quadratic Gaussian grid, and with 47 model layers in the vertical. The uppermost layer is located around 0.01 hPa. The time step was set to 720 s and the time interval for the output data to 6 h.

The basic submodels for dynamics, clouds, and diagnostics (see Table A1 in the appendix and Jöckel et al. 2005, 2010, 2016 for more information on these submodels) are applied for this study. For radiation the combined RAD and FUBRAD scheme is used. This is a parameterization to calculate the shortwave heating rates with an increased spectral resolution for solar variability studies. It replaces the default RAD radiation at wavelengths most sensitive to solar radiation in the UV and visible) between the model top and 70 hPa (Nissen et al. 2007; Dietmüller et al. 2016). Tropical winds were nudged to resemble the quasi-biennial oscillation (QBO), with a relaxation time of 60 days.

With the above described EMAC model setup without interactive chemistry, three different simulations were performed: a preindustrial (pi) control simulation (piCtrl), a 4-times CO₂ control simulation (4xCO₂Ctrl), and a 4-times CO₂ simulation with preindustrial ozone mixing ratios (4xCO₂piO₃). The chemical species and sea surface conditions are prescribed from a set of pi-control and 4xCO₂ simulations with a fully coupled chemistry-climate EMAC model version with coupled ocean, which were performed in accordance with the CMIP6 protocol (Eyring et al. 2016). Since our interest is to analyze the effect of ozone changes on stratospheric circulation, we prescribe the ozone fields, and additionally prescribe sea surface conditions to exclude the effects of stratospheric ozone feedbacks on surface temperature changes. This approach allows for a clean quantification of the effects of CO₂-induced ozone changes for the equilibrium climate states, but not for any nonlinear evolving transient feedbacks on different time scales. The approach is valid as long as the temperature and circulation response in the fully coupled model simulations (from which the ozone fields are taken) are reproduced by the simulations with prescribed ozone, and the respective figures are shown in the online supplement (Figs. S7–S9). The response in temperature and circulation are qualitatively similar between the fully coupled and the prescribed simulations, but there are some quantitative differences. Those likely stem from differences in

the details of the setup of the simulations, but we consider them small enough so that the ozone changes from the fully coupled simulations still are consistent with the circulation changes in the simulation with prescribed ozone.

Specifically, in all simulations, the sea surface temperatures (SSTs) and sea ice concentrations (SICs) are prescribed to 30-yr SST and SIC climatologies of the coupled EMAC CMIP6 pi-control and 4xCO₂Ctrl simulations, respectively. Note that the 30-yr climatologies are calculated over years 120–150 after the start of the 4xCO₂ forcing.

Zonally averaged, multiannual, monthly climatologies of ozone (O₃), N₂O, and CFCs are prescribed from the coupled EMAC CMIP6 simulations for the radiation scheme. Note that a zonal averaged ozone and not a 3D ozone field is used for better comparison with other studies (e.g., Chiodo and Polvani 2019). All these climatologies were generated from the last 30 years of 150 yearlong simulations to assure that the climate state is largely in equilibrium. Methane (CH₄) oxidation, an important source of stratospheric water vapor (le Texier et al. 1988; Eichinger et al. 2015; Frank et al. 2018), is calculated by the CH₄ submodel (Winterstein and Jöckel 2021) with prescribed zonally averaged, multiannual, monthly climatologies of OH, Cl, and O(¹D) from the coupled EMAC CMIP6 simulations. CO₂ and CH₄ are treated as tracers in the simulations, of which the lower boundary conditions are prescribed (by Newtonian relaxation with the submodel TNUDGE; Kerkweg et al. 2006) with year 1850 conditions from the datasets that were also used for the coupled EMAC CMIP6 simulations. For the 4xCO₂ simulations, the CO₂ mixing ratio of the lower boundary condition is quadrupled. Other than the simplified methane oxidation scheme, no (interactive) chemistry is activated in the simulations. The simulations cover 60 years; however, the first 10 years are considered as spinup and only the 50 years after the spinup time were analyzed.

As mentioned above, the simulations use a prescribed ozone field from the EMAC CMIP6 simulations. Ozone from the pi-control CMIP6 simulation is applied in the piCtrl and in the 4xCO₂piO₃ simulation and the ozone field from the CMIP6 4xCO₂ simulation is applied in the 4xCO₂Ctrl simulation. Note that since the prescribed ozone fields are taken from simulations with interactive chemistry, all circulation changes caused by ozone are included in the ozone fields. Figure 1 illustrates the relative difference of the ozone fields between the CMIP6 4xCO₂ and piCtrl simulations. In the 4xCO₂ simulation, ozone in the lower tropical stratosphere is lower and ozone in the extratropical and upper stratosphere is higher. This is in line with previous studies (Nowack et al. 2018; Chiodo and Polvani 2017; Chiodo et al. 2018; Chiodo and Polvani 2019).

b. Analysis methods

The results of these simulations are analyzed to investigate the impact of ozone changes on the temperatures and circulation. The difference between the results of the 4xCO₂Ctrl and the piCtrl simulation describes the change due to 4xCO₂ for which ozone adapts to the new climate state (i.e., with a prescribed ozone field from a 4xCO₂ coupled EMAC CMIP6 simulation) and is abbreviated as $\Delta\text{CO}_2^{\text{Ctrl}}$. The effect of the ozone changes

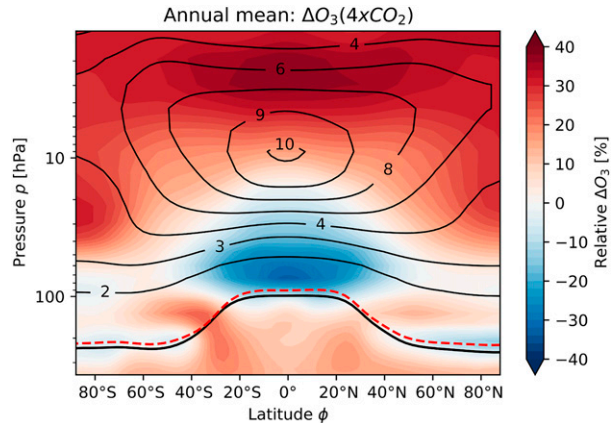


FIG. 1. Relative difference between prescribed ozone field used in this study for 4xCO₂ conditions and preindustrial (pi) conditions $\{[\text{O}_3(4\text{xCO}_2) - \text{O}_3(\text{pi})]/\text{O}_3(\text{pi})\}$; colors. This shows the relative ozone response of 4xCO₂. Solid contours depict the molar mixing ratio of ozone ($\mu\text{mol mol}^{-1}$) for pi conditions. The black line marks the pi-control tropopause and the red dashed line marks the 4xCO₂ tropopause.

due to 4xCO₂ is calculated by the difference between the 4xCO₂ simulation with adapted ozone (4xCO₂Ctrl) and the 4xCO₂ simulation in which ozone is held constant at preindustrial levels (4xCO₂piO₃) and is abbreviated as ΔO_3 in the following. The calculation of various diagnostics used for the analysis are described in the following.

The residual mass streamfunction $\hat{\psi}$ represents the net meridional overturning mass transport and is calculated by

$$\hat{\psi} = 2\pi r_0 \cos(\varphi) g^{-1} \int_p^0 \bar{v}^* dp, \quad (1)$$

where r_0 is Earth's radius, φ is the latitude, g is the gravitational acceleration, p is the pressure, and \bar{v}^* is the zonal mean of the meridional residual velocity, which is calculated by the transformed Eulerian mean (TEM) equations (Andrews et al. 1987).

The BDC describes tracer transport in the stratosphere. One way of diagnosing tracer transport is the average age of an air parcel moving through the stratosphere. This is called the mean age of air (AoA). The AoA in units of time has to be derived from tracer measurements. To obtain AoA from the model a so-called “clock tracer” (Hall and Plumb 1994; Waugh and Hall 2002) is implemented, which is an inert tracer with a mixing ratio that linearly increases over time as lower boundary condition. AoA is then calculated as the time lag between the current local mixing ratio at a certain grid point and the same mixing ratio at the boundary layer, i.e., measures the time an air parcel travels from the boundary layer to this grid point.

As described above, the BDC is forced by dissipating atmospheric waves. The vertical component of the EP fluxes represents vertical propagation of planetary and synoptic-scale waves. EP fluxes and their divergence are calculated following Andrews et al. (1987). The components of the EP fluxes are given in spherical coordinates F_φ and F_p . For scaling the EP fluxes and their arrows for illustration purposes

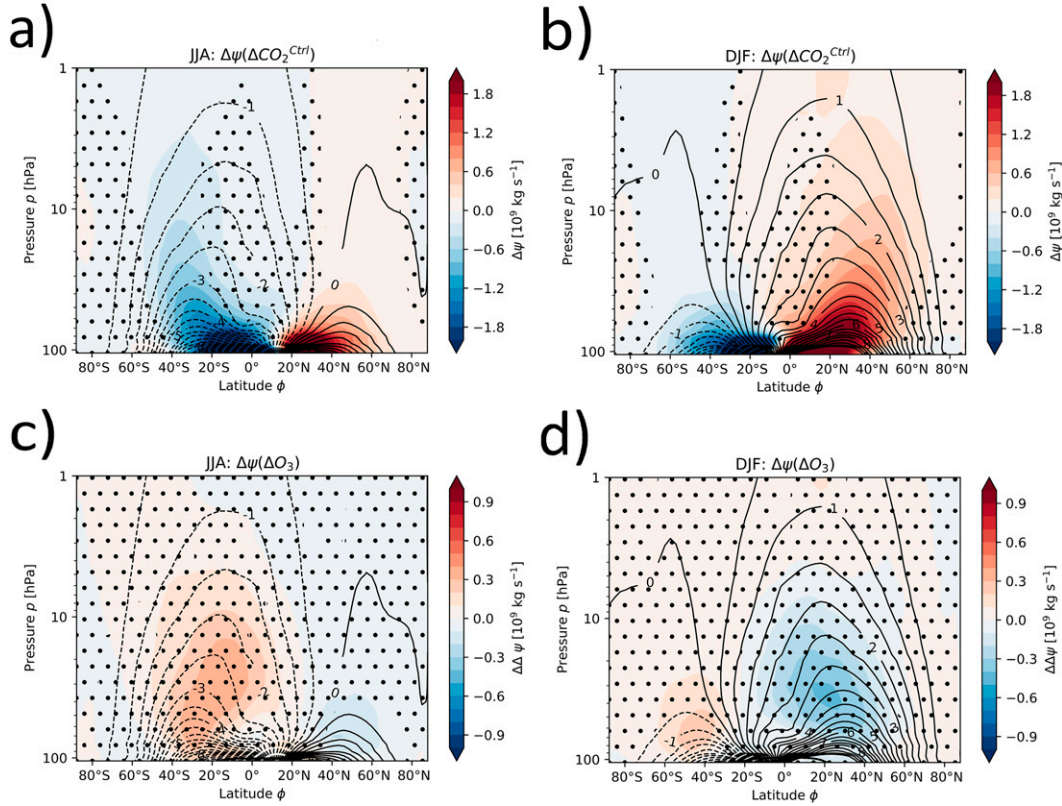


FIG. 2. Response of streamfunction ψ (colors) to (a),(b) $\Delta\text{CO}_2^{\text{Ctrl}}$ and (c),(d) ΔO_3 for (left) JJA and (right) DJF. Contours depict ψ of the piCtrl simulation in 10^9 kg s^{-1} . Nonsignificant responses at the 95% confidence level are stippled. Note that the scaling of the color bar is different between $\Delta\text{CO}_2^{\text{Ctrl}}$ and ΔO_3 .

(see Fig. 7), whose horizontal and vertical components are proportional to each other, we use following formulas:

$$\hat{F}_\varphi = 2\pi r_0 g^{-1} \cos^2 \varphi F_\varphi, \quad (2)$$

$$\hat{F}_p = 2\pi r_0^2 g^{-1} \cos^2 \varphi F_p 100^{-1}, \quad (3)$$

are used, similarly to Eq. (3.13) by Edmon et al. (1980) and to Table 2 in Jucker (2021). The division of the vertical component F_p through the whole vertical (pressure) domain by 100 is needed to convert the unit from $\text{m}^3 \text{ Pa}$ to $\text{m}^3 \text{ hPa}$. The unit of the horizontal component F_p is m^3 after the scaling.

According to the downward control principle (Haynes et al. 1991), the wave forcing \bar{F} above a certain pressure level drives the residual meridional overturning circulation. This is expressed as the streamfunction (Okamoto et al. 2011):

$$\Psi(\varphi, p) = \frac{\cos \varphi}{g} \int_p^0 \bar{F} dp, \quad (4)$$

for steady state with \hat{f} given by

$$\hat{f} = f - \frac{1}{r_0 \cos \varphi} \left[\frac{\partial(\bar{u} \cos \varphi)}{\partial \varphi} \right] = 2\Omega \sin \varphi - \frac{1}{r_0} \frac{\partial \bar{u}}{\partial \varphi} + \frac{\bar{u} \sin \varphi}{r_0 \cos \varphi}. \quad (5)$$

The above expression allows us to quantify the residual circulation (changes) driven by the sum of total resolved and unresolved wave forcing (changes), with $\bar{F} = [1/(\rho_o r_o \cos \varphi)] \nabla \cdot \mathbf{F} + \bar{X}$ (where ρ_o is the basic state air density, $\nabla \cdot \mathbf{F}$ is the divergence of the Eliassen–Palm flux, and \bar{X} represents the gravity wave drag).

The impacts of the 4xCO₂ and of the CO₂-induced ozone changes on the different variables are also statistically analyzed. For this purpose, a two-sided Student's *t* test is applied. In the figures that are shown in sections 3 and 4, the differences are considered to be statistically significant if the confidence level exceeds 95%.

3. Effects on the Brewer–Dobson circulation (BDC)

The response of the residual mass streamfunction to $\Delta\text{CO}_2^{\text{Ctrl}}$ (Figs. 2a,b) and to ΔO_3 (Figs. 2c,d) for JJA and DJF is illustrated in Fig. 2, based on the simulations described in section 2.

Higher CO₂ mixing ratios robustly increase the total values of the mass streamfunction in both hemispheres (Figs. 2a,b), especially in the midlatitudes and in the lower tropical stratosphere. These higher values of the mass streamfunction indicate the well-known global strengthening of the residual circulation in response to CO₂ forcing (e.g., Garcia and Randel 2008; Abalos et al. 2021; McLandress and Shepherd 2009).

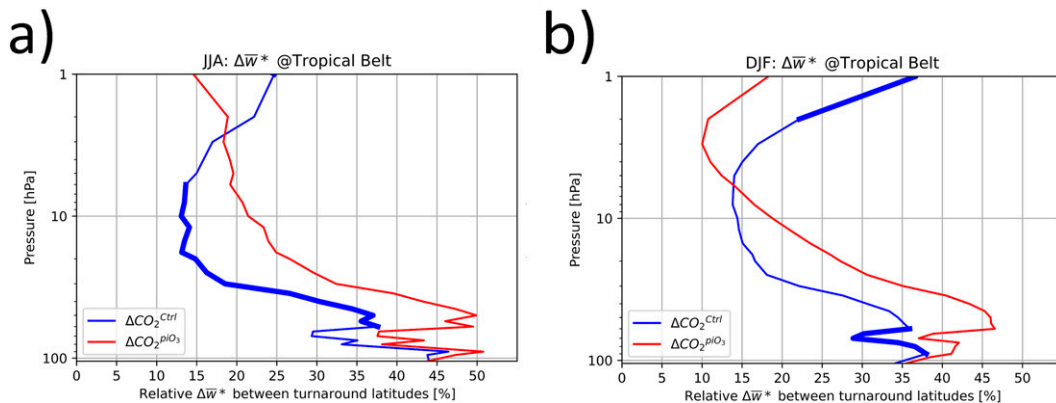


FIG. 3. Relative response of the total tropical upwelling as average residual velocity \bar{w}^* between the turnaround latitudes in the tropics to $\Delta\text{CO}_2^{\text{Ctrl}}$ (blue) and to $\Delta\text{CO}_2^{\text{piO}_3}$ (red). This is shown as function of pressure for (a) JJA and (b) DJF. The pressure altitudes where the differences between $\Delta\text{CO}_2^{\text{Ctrl}}$ and $\Delta\text{CO}_2^{\text{piO}_3}$ are statistically significant at the 95% confidence interval are marked with a thick blue line. Note that the turnaround latitudes mark the latitudes where \bar{w}^* turns from positive to negative values.

The CO_2 -induced ozone changes lead to a systematic decrease of the mass streamfunction in both hemispheres, mostly counteracting the CO_2 -induced acceleration of the BDC. However, due to large internal variability most of these ozone-induced changes are not statistically significant for the given length of record, except within the shallow branch of the BDC during summer (Figs. 2c,d).

The systematic change of the residual mass streamfunction is also reflected in the total tropical upwelling strength as shown in Fig. 3. Quadrupling of CO_2 enhances tropical upwelling in JJA as well as in DJF at all altitudes in the lower stratosphere by up to 50%, if ozone is held fixed in preindustrial conditions (see Fig. 3a, red line). This is qualitatively consistent with the well-known trends in residual mean vertical velocity caused by increased GHG concentrations (e.g., Li et al. 2008; Garcia and Randel 2008). When scaling with the global mean warming, the increase of \bar{w}^* in the tropics by $5\% \text{ K}^{-1}$ at 10 hPa and $8\% \text{ K}^{-1}$ at 70 hPa is quantitatively consistent with the results from the studies by Chrysanthou et al. (2020) and Abalos et al. (2021), who quantified these values to be $6\% \text{ K}^{-1}$ at 10 hPa and $9\% \text{ K}^{-1}$ at 70 hPa as well as between 5% and $13\% \text{ K}^{-1}$ (depending on the model) at 70 hPa, respectively.

In both seasons, tropical \bar{w}^* weakens in the tropics by up to 15% through ΔO_3 in the lower and middle stratosphere (cf. blue versus red lines in Fig. 3). This effect is statistically significant in DJF, between 90 and 60 hPa, where the shallow BDC branch is located, and in JJA extending up to 5 hPa. DallaSanta et al. (2021) found an ozone-induced $\sim 10\%$ – 20% decrease of upwelling in the inner tropics (10°N – S , see their Fig. 6) between about 70 to 10 hPa, which is quantitatively consistent with our results. However, they find no response of ozone below 70 hPa, and it is unclear whether this is due to differences in the diagnostic (inner tropics versus entire tropics) or a model sensitivity. In the upper stratosphere, we find a 10% – 15% increase in tropical upwelling due to ozone changes during DJF and less so in JJA. This relatively enhanced upwelling is consistent with the systematic strengthening of the residual circulation in the upper stratosphere in winter (see Fig. 2d).

The mass streamfunction (Fig. 2) and tropical \bar{w}^* (Fig. 3) only describe the net mass transport contribution to the BDC, not including two-way mixing that does not involve net mass exchange (Garny et al. 2014; Dietmüller et al. 2017, 2018; Eichinger et al. 2019). AoA appropriately reflects both of these transport contributions. The changes of AoA due to $\Delta\text{CO}_2^{\text{Ctrl}}$ are shown in Figs. 4a and 4b, and the changes due to ΔO_3 are shown in Figs. 4c and 4d.

Quadrupling of CO_2 leads to an AoA decrease between 0.5 years in the tropical lower stratosphere and 1.5 years in the extratropical stratosphere (Figs. 4a,b). This is in line with the enhancement of the BDC strength due to higher CO_2 mixing ratios that strengthens meridional tracer transport (e.g., Butchart and Scaife 2001; Garcia and Randel 2008). The non-uniform changes of AoA are caused by quasi-horizontal mixing processes (Garny et al. 2014).

The CO_2 -induced ozone changes alone lead to increased AoA (Figs. 4c,d) throughout the stratosphere in winter and summer, which results in a damping of the CO_2 effect by up to 23% in DJF. These AoA modifications are consistent with the corresponding modifications of the residual circulation, although they are statistically more robust (more wide spread coverage of statistically significant values compared to Figs. 2c,d). This is likely because AoA displays the spatial and temporal integral of the circulation strength along the path of an air parcel (Hall and Plumb 1994).

4. Mechanisms of the BDC decrease by ozone changes

The CO_2 -induced ozone changes modify the radiative heating rates locally in the stratosphere, with increased/reduced ozone abundances leading to enhanced/reduced radiative heating (see Fig. S1).

The radiative effects directly influence the temperature field, providing the mechanistic starting point of circulation changes in our model simulations. Figure 5 illustrates the resulting temperature response for $\Delta\text{CO}_2^{\text{Ctrl}}$ (Figs. 5a,b) and for ΔO_3 (Figs. 5c,d), both for JJA and DJF.

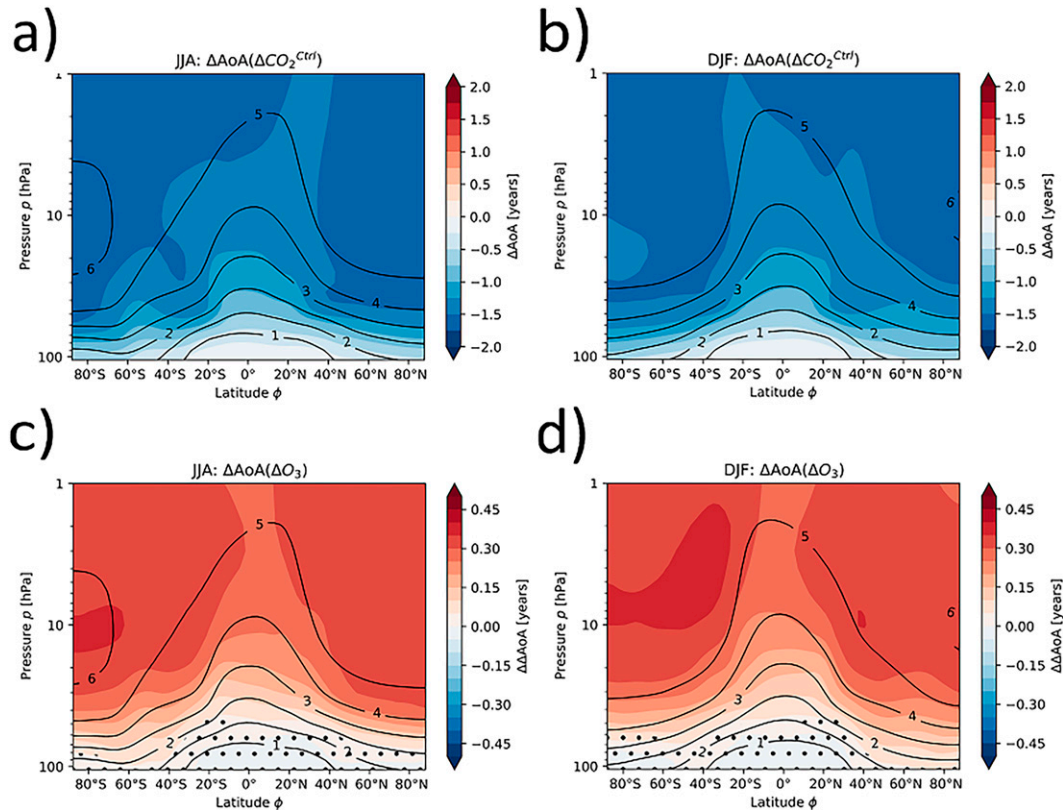


FIG. 4. Response of age of air (AoA; colors) to (a),(b) $\Delta\text{CO}_2^{\text{Ctrl}}$ and (c),(d) ΔO_3 for (left) JJA and (right) DJF. Contours depict the AoA of the piCtrl simulation in years. Nonsignificant responses at the 95% confidence level are stippled. Note that the scaling of the color bar is different between $\Delta\text{CO}_2^{\text{Ctrl}}$ and ΔO_3 .

The increased CO₂ concentrations lead to the well-known warming of the troposphere (here by up to 8 K) and cooling of the stratosphere (here by more than 12 K), consistent with previous 4xCO₂ experiments (IPCC 2018).

The CO₂-induced ozone changes lead to a warming in the upper stratosphere in the tropics and extratropics, linked to strong absorption of shortwave radiation (see Figs. S1c,d) due to increased ozone (see Fig. 1). In the upper stratosphere, the maxima reach up to 3–5 K, and warming is more pronounced in the respective summer hemisphere, consistent with availability of shortwave radiation (see Figs. 5c,d). In the tropical lower stratosphere, temperatures decrease by about 2 K, consistent with decreasing ozone abundances in this region. In the summer middle stratosphere, the temperature increases by about 2 K over both polar caps. Over Antarctica statistically significant warming appears also in the lowermost stratosphere (around 150 hPa). These temperature changes are quantitatively similar to those described in the studies by Chiodo and Polvani (2019) and Nowack et al. (2015). Note at this point that also changes in stratospheric water vapor play a role in terms of radiative heating (see e.g., Maycock et al. 2014), which is further discussed in section 6.

The temperature changes shown in Figs. 5c and 5d are induced by the prescribed ozone changes, but next to the direct radiative effects they also include any circulation effects on

temperatures, complicating the causal attribution. However, the pattern of temperature changes is largely consistent with expected radiative effects of the prescribed ozone differences (see also Yook et al. 2020; Ivanciu et al. 2022). We will therefore assume in the following that the modified circulation response due to the ozone differences may be explained by the altered temperature gradient in the lower stratosphere caused by radiative effects, and its associated altered vertical wind shear.

The larger amount of CO₂ in $\Delta\text{CO}_2^{\text{Ctrl}}$ strengthens the subtropical jets (STJs) by more than 10 m s^{−1} and shift them upward (Figs. 6a,b), consistent with previous studies (e.g., Vallis et al. 2015; Oberländer-Hayn et al. 2016; Chiodo and Polvani 2019; Eichinger and Sacha 2020; Pisoft et al. 2021) and consistent with the meridional temperature gradient described above. Moreover, the easterlies in summer are robustly weakened by thermal effects (see Figs. 6a,b). The Antarctic polar vortex strengthens through an increase of CO₂, which is in balance with a strengthening of the meridional temperature gradient in the lower stratosphere in the austral winter hemisphere (Fig. 6a). The weakening of the Arctic polar vortex lies within the large envelope of the simulated response of the Arctic vortex to CO₂ increases, with some models showing a decrease and some an enhancement of the vortex strength (see e.g., Karpechko et al. 2022). Next to the stratospheric wind changes, the well-known CO₂-induced poleward shift of the tropospheric austral EDJ is

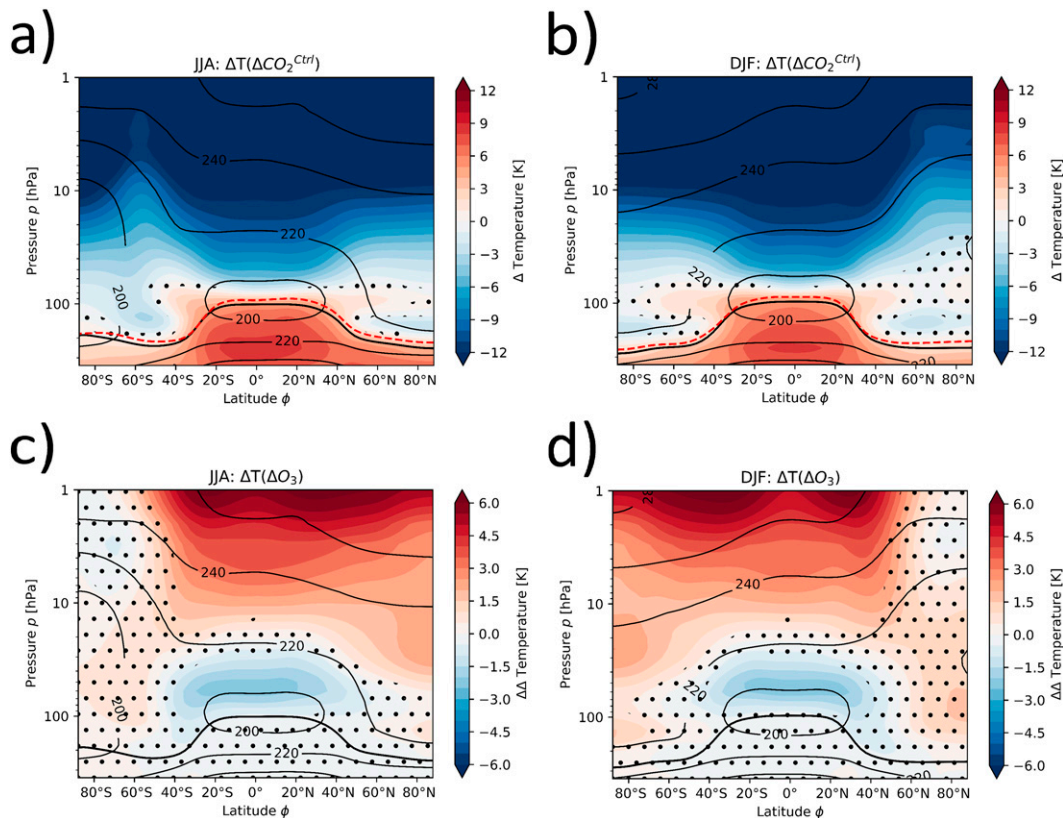


FIG. 5. Response of temperature (colors) to (a),(b) $\Delta 4\times\text{CO}_2^{\text{Ctrl}}$ and (c),(d) ΔO_3 for (left) JJA and (right) DJF. The black thick line illustrates the tropopause, and the contours depict the temperature (K) of the piCtrl simulation. The red dashed line in (a) and (b) marks the tropopause for $4\times\text{CO}_2$ conditions. Nonsignificant responses at the 95% confidence level are stippled. Note that the scaling of the color bar is different between $\Delta\text{CO}_2^{\text{Ctrl}}$ and ΔO_3 .

evident, especially in summer (see also Fig. S5). The stronger poleward shift is possibly in parts linked to the downward extent of the weakened stratospheric easterlies to the troposphere (see Fig. S3), which was shown in the studies by Byrne et al. (2017), Byrne and Shepherd (2018) and Ceppi and Shepherd (2019).

The $4\times\text{CO}_2$ -induced ozone changes (ΔO_3 , see Figs. 6c,d) also modify the zonal wind in the stratosphere of the summer hemisphere, strengthening the easterlies in the middle and upper stratosphere by up to 3 m s^{-1} . The stronger easterlies in summer are consistent with the increased meridional temperature gradient in the lower stratosphere caused by the radiative effects of ozone changes, which is also in line with the results of Chiodo and Polvani (2019).

The zonal wind changes further modify the propagation conditions for planetary and synoptic-scale waves. As shown in Figs. 7a and 7b the convergence of the EP flux at the upper flanks of the STJ is increased, caused by an upward shift of the critical lines for wave dissipation (Shepherd and McLandress 2011). In addition to that, wave forcing increases (more negative EPFD) in the vicinity of the Arctic polar vortex in northern winter, consistent with the decrease in the polar vortex strength (Fig. 7b). The enhanced wave breaking at the STJs and at the Arctic polar vortex strengthens the BDC (see Figs. 2a,b).

The $4\times\text{CO}_2$ -induced ozone effects lead to more vertical planetary wave propagation at the Antarctic polar vortex (Fig. 7c) and to less equatorward wave deflection at the Arctic polar vortex (Fig. 7d). This weakens the polar vortices and hence strengthens their radiatively induced seasonal breakdown, in particular in the Antarctic. Moreover, the corresponding enhanced but not significant wave breaking in the vicinity of the polar vortices (not shown) systematically strengthens the residual flow in the winter upper stratospheres (see Figs. 2c,d).

A positive change of the mean flow strengthening by EPFD (i.e., decrease in wave forcing in response to ozone) that is statistically significant is found above about 70 hPa in the summer hemisphere. This decrease in wave forcing is understood given the decrease in the zonal mean zonal winds in the summer stratosphere forced by the ozone changes: While the CO_2 -forcing shifts the critical lines for wave breaking upward, ozone counteracts this effect and attenuates vertical wave propagation (see Figs. 7c,d). This leads to less wave breaking in the lower stratosphere above the STJ, and thereby to a decrease in the wave driving of the shallow BDC branch (see Figs. 2c,d). The effects of altered wave forcing on the residual circulation is quantified by the downward control method as outlined in section 2b.

The BDC is also driven by breaking gravity waves that in our model are represented by the parameterized gravity wave

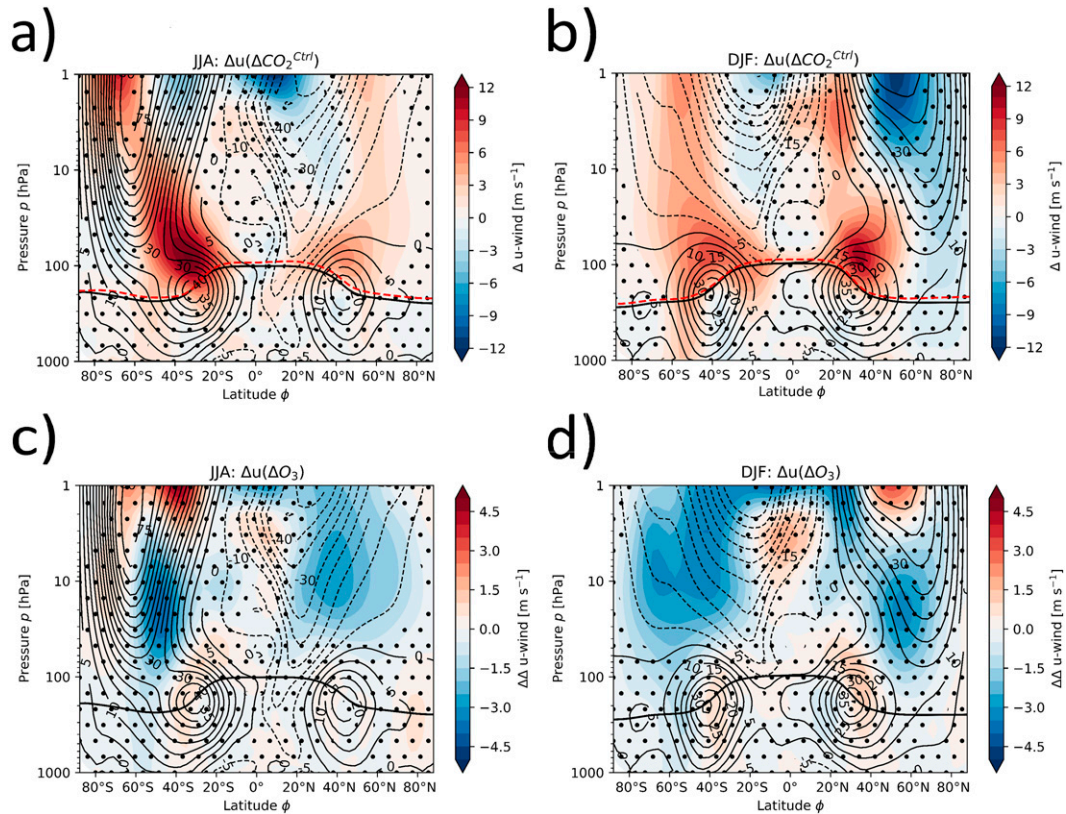


FIG. 6. Response of zonal wind (colors) to (a),(b) $\Delta 4xCO_2^{Ctrl}$ and (c),(d) ΔO_3 for (left) JJA and (right) DJF. The black thick line illustrates the tropopause, and the contours depict the zonal wind ($m s^{-1}$) of the piCtrl simulation. The red dashed line in (a) and (b) marks the tropopause for $4xCO_2$ conditions. Nonsignificant responses at the 95% confidence level are stippled. Note that the scaling of the color bar is different between ΔCO_2^{Ctrl} and ΔO_3 .

drag (GWD). The effects of GWD and EPFD on the residual circulation changes at 70 hPa calculated via the method of downward control are shown in Fig. 8.

These results underline the strengthening of the residual circulation in the lower stratosphere through ΔCO_2^{Ctrl} as well as the damping of this CO_2 -induced acceleration through ΔO_3 , which is forced by atmospheric wave breaking. In the summer shallow branch, the damping by ΔO_3 amounts to about 20% of the CO_2 -induced acceleration. In winter, the decrease in the absolute residual circulation strength is of similar absolute magnitude than in summer. Additionally, Fig. 8 also shows the role of the EPFD as the main factor in the changes in the shallow BDC branches. Note that there is a substantial deviation between the response of ΔO_3 calculated by the sum of all types of wave forcing and the response of ΔO_3 calculated by the TEM equations in Fig. 8d. This is likely caused by the fact that the absolute response of the residual mass streamfunction to ΔO_3 itself is small.

The relative contribution of OGWD and resolved wave drag to positive trend in the residual circulation in Figs. 8a and 8b varies substantially among models (Butchart et al. 2010). As OGWD is identified as the main driver of the positive trend, however, with latitudinal and hemispheric dependence. We note that OGWD driving does not support the damping between 20° and 40°N/S due to the zonal wind strengthening in

the lower stratosphere (Li et al. 2008). Overall, this may be sensitive to intermodel differences in the OGWD parameterization (McLandress and Shepherd 2009).

5. Effects on the polar vortices

Figures 6c and 6d show a systematic attenuation of the polar vortices due to CO_2 -induced ozone changes. Moreover, the stratospheric easterlies in summer strengthen in response to the ozone changes, indicating a shorter polar vortex season. For a more detailed analysis of these effects, the climatological zonal mean zonal wind of 60°N/S and at 10 hPa are shown in Fig. 9, which is a common diagnostic for the polar vortex strength (see e.g., Charlton and Polvani 2007; Baldwin et al. 2021).

For preindustrial conditions the polar vortex turns westerly in early August in the NH and mid of March in the SH. The breakdown takes place at the end of March in the NH and at the end of October in the SH. In the $4xCO_2$ simulations ($4xCO_2^{Ctrl}$ and $4xCO_2^{piO_3}$) the polar vortex formation starts earlier and the breakdown occurs later, which is in line with the study by Ayarzagüena et al. (2020). This means that the period of the polar vortex is longer due to an increase of CO_2 (see also Figs. S3a,b). Moreover, the SH polar vortex is systematically stronger in the $4xCO_2$ simulations.

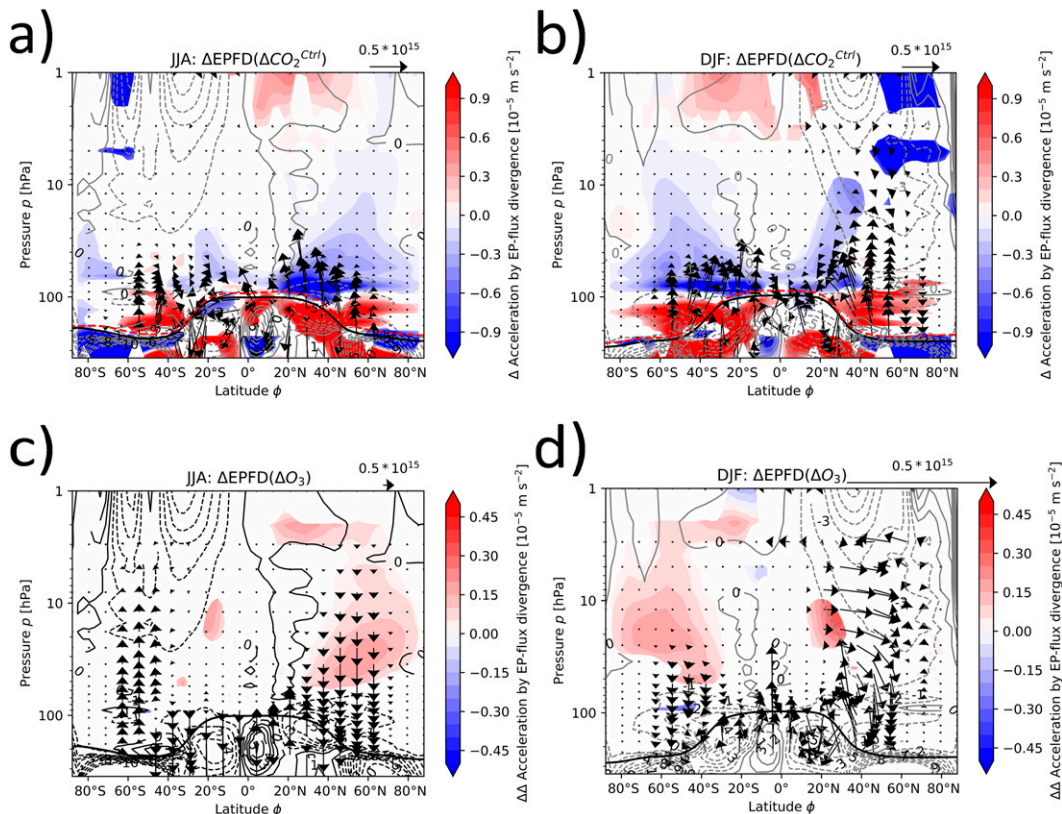


FIG. 7. Response of EPFD (colors) and EP flux (arrows) to (a),(b) $\Delta 4xCO_2Ctrl$ and (c),(d) ΔO_3 . Note that for EPFD only the significant responses on the 95% confidence level are illustrated. The responses are shown for (left) JJA and (right) DJF. The contours depict the EPFD of the piCtrl simulation. The black line marks the pi-control tropopause, and the red dashed line marks the $4xCO_2$ tropopause. Note, unit of the quantity for the horizontal/vertical EP flux component is $m^3 m^{-3} hPa^{-1}$, and that the scaling of the color bar is different between ΔCO_2^{Ctrl} and ΔO_3 .

Due to CO_2 -induced ozone changes, the NH polar vortex is only systematically enhanced at the beginning and at the end of the period (August–September and February–April). From November until January, the NH polar vortex is systematically weaker in $4xCO_2Ctrl$. However, the standard deviation (blue shading) is larger than the differences between the $4xCO_2$ simulations. In the $4xCO_2Ctrl$ simulation, the polar vortex builds up later and breaks down earlier than in the $4xCO_2piO_3$ simulation. Note also that the final warming itself happens more abruptly if ozone is changed through $4xCO_2$ (as illustrated in Fig. S6 that shows the anomaly of the polar cap geopotential height at 10 hPa relative to the final warming date for all three simulations).

Figure 9 indicates that an increase of CO_2 leads to a later vortex breakdown, also known as final warming. The ozone changes, in contrast, lead to an earlier vortex breakdown. The distribution of the final warming dates over all individual years of the simulations is shown in Fig. 10.

Quadrupling of the CO_2 concentration postpones the climatologically averaged final warming in the NH by 4 days (see Figs. 10a,b). Moreover, the spread of the final warming date distribution in this hemisphere is reduced if the amount of CO_2 in the simulation is higher. In the SH, a shift of the final warming

to a later date is even more evident (see Figs. 10d,e). On average, the final warming takes place 8 days later in $4xCO_2Ctrl$ in the SH. The median of the $4xCO_2Ctrl$ distribution is similar to the 75th percentile of the piCtrl distribution indicating robustness of the delayed vortex breakdown in the SH.

The ozone changes through $4xCO_2$ shift the distribution to earlier dates in both hemispheres. In the climatological mean, the final warming occurs 5 days earlier in the NH and even 7 days earlier in the SH in the $4xCO_2$ simulation with changed ozone in comparison to the $4xCO_2$ simulation with unchanged (preindustrial) ozone. In other words, without ozone changes through $4xCO_2$, the shift of the final warming dates in a $4xCO_2$ simulation would be around 2 times larger. Note, that in the SH the shift between piCtrl and $4xCO_2Ctrl$ is 7 days and between piCtrl and $4xCO_2piO_3$ it is 15 days. In the SH, the 75th percentile of the distribution in the simulation with changed ozone ($4xCO_2Ctrl$) is equal to the median of the distribution in the simulation with unchanged preindustrial ozone (see Figs. 10e,f).

The impacts of CO_2 -induced ozone changes on the stratospheric zonal winds, and in particular on the vortex breakdown date is expected to alter the tropospheric jets via stratosphere–troposphere downward coupling (see e.g., Byrne and Shepherd 2018; Ceppi and Shepherd 2019). Figures 6c

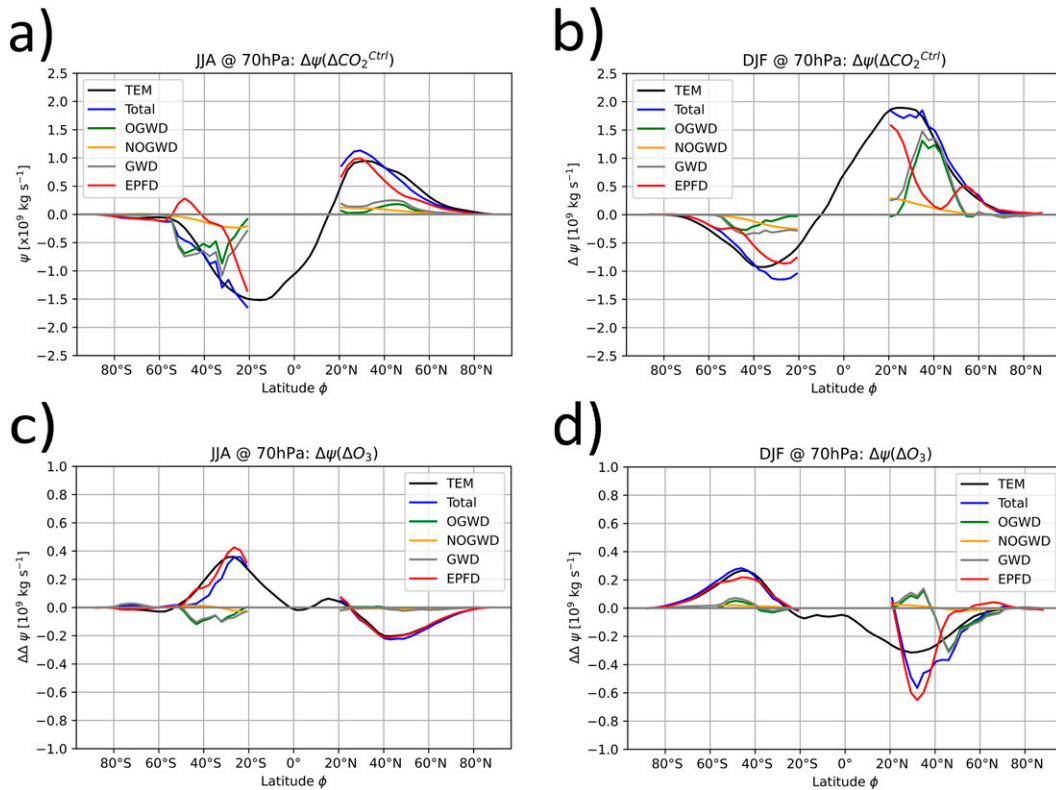


FIG. 8. Response of mass streamfunction to (a),(b) $\Delta\text{CO}_2^{\text{Ctrl}}$ and (c),(d) ΔO_3 . This is shown for (left) JJA and (right) DJF at 70 hPa as a function of latitude. The streamfunction is calculated via the TEM equations (TEM; black) and with the downward control method for EPFD (red) and GWD (gray), which is the sum of OGWD (green) and NOGWD (yellow). The sum of all these wave forcings (Total = EPFD + GWD) is represented as a blue line.

and 6d depict that the ozone induced changes of the stratospheric polar vortices and easterlies in the SH extend down to the poleward flank of the EDJ. The negative change of the zonal wind of the poleward EDJ flank indicates a weakening of the poleward EDJ shift in $\Delta\text{CO}_2^{\text{Ctrl}}$. The stratospheric negative zonal wind anomaly extends downward especially in the SH midlatitudes at the end of the vortex season (see

Figs. S3c,d). At this time, the decelerated polar vortex systematically weakens the EDJ (see Fig. S4) and influences its position, albeit those changes are not statistically significant in our model simulations. The CO_2 -induced poleward shift is systematically damped in the SH (see Fig. S5). Thus, our model simulations confirm the results by Nowack et al. (2018) and Chiodo and Polvani (2019) on the role of ozone changes

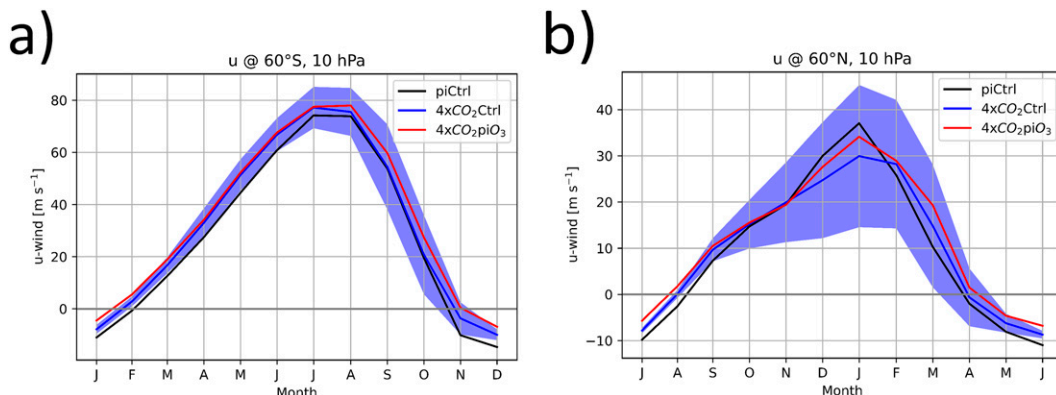


FIG. 9. Climatological zonal mean zonal wind at 10 hPa and (a) 60°S and (b) 60°N for the piCtrl (black), 4xCO₂Ctrl (blue), and 4xCO₂piO₃ simulations (red). The standard deviation of the 4xCO₂Ctrl simulation is shown as blue shading.

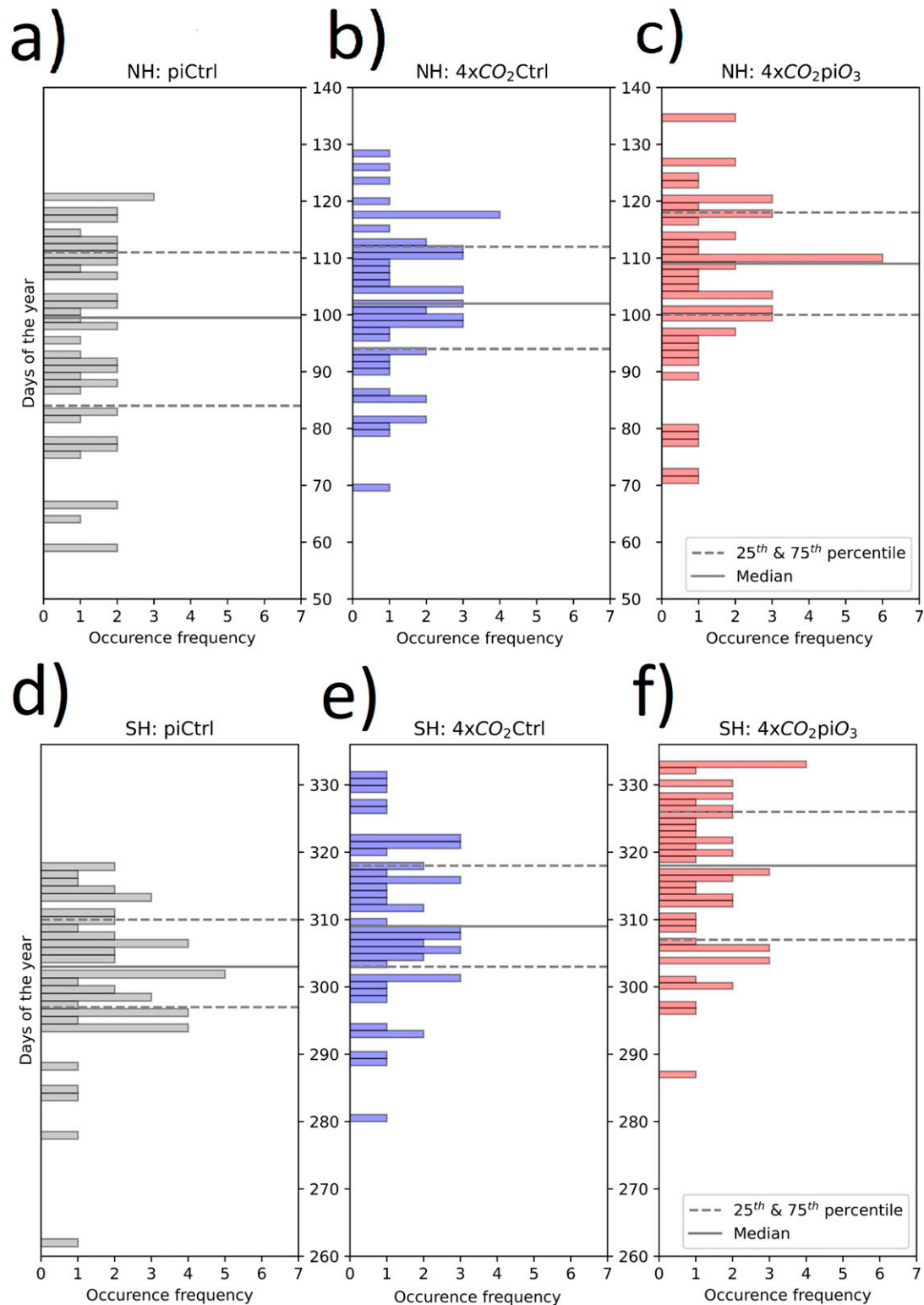


FIG. 10. Distributions of the stratospheric final warming dates for the piCtrl, 4xCO₂Ctrl, and 4xCO₂piO₃ simulations in the (a)–(c) NH and (d)–(f) SH. The gray dashed lines depict the 25th and 75th percentiles. The gray solid lines denote the medians.

in damping the CO₂-induced poleward EDJ shift, even though those changes are not significant in statistical terms in our model. In general, the link between the stratospheric final warming date and the position of the tropospheric EDJ in the following month is consistent with a number of recent studies (Ceppi and Shepherd 2019; Mindlin et al. 2021).

6. Discussion

We performed dedicated simulations with the EMAC model to investigate the impact of CO₂-induced ozone changes on the equilibrated stratospheric circulation response to 4xCO₂, with particular emphasis on the BDC, and analyzed the mechanism responsible for ozone-induced BDC changes. To quantify the effects of CO₂-induced ozone changes, we performed a set of pi-control and 4xCO₂ simulations, in which prescribed ozone concentrations were either adapted to the new climate state, or held constant at pi-control conditions.

A key result revealed by our set of simulations is the fact that CO₂-induced ozone changes lead to a statistically significant damping of the BDC strengthening, which means that the ozone changes act as negative feedback on the circulation. The damping of the residual circulation along the shallow branch in summer is as strong as 20% of the total change and is statistically significant at the 95% confidence level. In the winter hemisphere, the relative damping is somewhat weaker and statistically not as robust. The damping of the CO₂-induced shallow branch acceleration is reflected in a statistically significant ozone-induced weakening of w^* in the lower stratosphere of around 20%. The damping of the residual circulation strengthening is further reflected in a robustly weaker AoA decrease throughout the entire stratosphere. The damped BDC strengthening is also apparent as a damping of the vertical residual velocity in the tropics, which is overall consistent with the study of DallaSanta et al. (2021). However, it remains to be shown how robust the result of the ozone-induced damping of the BDC strengthening is across different models and model setups.

The starting point for the mechanism of the weakening of the CO₂-induced BDC acceleration are the thermal effects of the CO₂-induced ozone changes on the meridional temperature gradient in the lower stratosphere. This is an effect of reduced radiative heating through decrease of ozone in the lower tropical stratosphere and enhanced radiative heating through increase of ozone in the extratropical and tropical upper stratosphere. While the overall temperature response is only in parts due to radiative effects (Dietmüller et al. 2014), the statistically significant temperature response pattern (see Fig. 5) is proportional to the ozone-induced absorption of short-wave radiation. Offline radiative calculations or dedicated model experiments would be necessary to quantify the temperature response that is directly attributed to the ozone changes in absence of dynamical heating/cooling. Further, such calculations could reveal the relative role of the weakened tropical lower stratospheric heating versus the enhanced extratropical heating in inducing the change in the meridional temperature gradient.

The radiative heating/cooling in the stratosphere might further be influenced by changes in the amount of stratospheric water vapor (see e.g., Maycock et al. 2013, 2014). The changes of ozone lead to a relative decrease of the specific humidity of around 15%–20% in the stratosphere (see Fig. S2b). Maycock et al. (2013) showed that a uniform increase in water vapor leads to changes in the circulation, namely, increases in the zonal mean wind in the lower stratosphere. Thus, the ozone-induced decrease of water vapor might contribute to the decrease in lower stratospheric winds as found here, and it remains to be quantified how large the contribution of water vapor changes to the dynamical changes, which are reported here, are. The effect of ozone changes on stratospheric water vapor was also found by Dietmüller et al. (2014) and Nowack et al. (2018), who explained it with a lower tropical cold point temperature. However, it is worth mentioning that the stratospheric water vapor in our 4xCO₂piO₃ simulation is probably affected by too high ozone mixing ratios in the upper tropical troposphere. Quadrupling of the CO₂ mixing ratio lifts the tropopause, but in our 4xCO₂piO₃ simulation the ozone distribution does not change. Therefore, the ozone mixing ratios in the upper troposphere are biased high, leading to too high temperatures in this region. This leads to a too warm tropical cold point, which causes an increased water vapor intrusion into the stratosphere. Furthermore, dedicated model experiments revealed a substantial impact of ozone transport at the tropical tropopause layer on the tropical cold point (e.g., Birner and Charlesworth 2017; Charlesworth et al. 2019). However, Nowack et al. (2018) found that the tropical tropopause bias was not the dominant factor for the stratospheric water vapor differences in these types of simulations. Additionally, in the present study the response of the temperature and of the zonal wind in the lower stratosphere is quantitatively consistent with those shown by Nowack et al. (2018), who use simulations with interactive ozone chemistry instead of prescribed ozone fields as in our simulations. This indicates that despite the use of prescribed ozone fields, as necessary for the disentanglement of the role of ozone changes, our results are unlikely to be falsified by the possible artifact around the tropopause.

The ozone-induced change of the radiative heating rates in the lower stratosphere is, via thermal wind balance, consistent with a weaker and less persistent polar vortex, especially in the SH. This negative wind anomaly in winter extends down to the troposphere and leads to a damping of the GHG-induced poleward shift of the EDJ. In the SH, the stratospheric easterlies strengthen with high statistical confidence due to stronger meridional temperature gradient in the lower stratosphere, induced by ozone radiative heating. In winter, the dominant zonal winds in the middle stratosphere are also affected by wave forcing: The polar vortices weaken systematically consistent with enhanced planetary wave breaking. This stronger wave forcing at the polar vortices results in a systematic enhancement of the residual circulation in the upper stratosphere. In contrast, the wave activity at the STJ is weakened by ozone changes, resulting in a damping of the CO₂-induced acceleration of the shallow BDC branch.

The mechanism for the effects of CO₂-induced ozone changes on the BDC are in parts similar to the well-known effects of

TABLE A1. List of MESSy submodels that are used for dynamics, clouds, and diagnostics in the simulations of our study.

Submodel	Description	Reference(s)
AEROPT	Aerosol optical properties	Dietmüller et al. (2016)
CLOUD	ECHAM5 cloud scheme as MESSy submodel	Roeckner et al. (2006, and references therein)
CLOUDOPT	Cloud optical properties	Dietmüller et al. (2016)
CONVECT	Convective parameterization	Tost et al. (2006)
CVTRANS	Convective tracer transport	Tost (2006)
E5DIFF	ECHAM5 vertical diffusion scheme as MESSy submodel	Roeckner et al. (2006, and references therein)
GWAVE	ECHAM5 gravity wave parameterization as MESSy submodel	Baumgaertner et al. (2013)
ORBIT	Earth orbital parameters as MESSy submodel	Roeckner et al. (2006, and references therein)
OROGW	ECHAM5 gravity wave parameterization as MESSy submodel	Roeckner et al. (2006, and references therein)
PTRAC	Define additional prognostic tracers via namelist	Jöckel et al. (2008)
QBO	Newtonian relaxation of quasi-biennial oscillation	Giorgetta and Bengtsson (1999), Jöckel et al. (2006)
SURFACE	ECHAM5 surface scheme as MESSy submodel	Roeckner et al. (2006, and references therein)
TNUDGE	Newtonian relaxation of species as pseudoemissions	Kerkweg et al. (2006)
TROPOP	Tropopause and other diagnostics	Jöckel et al. (2006)
VAXTRA	Vertical axes transformations (for output)	Unpublished

CFC-induced Antarctic ozone depletion on the BDC (e.g., Abalos et al. 2019). In both cases, stratospheric ozone changes induce modifications of the meridional temperature gradient locally through radiative heating by ozone. However, in the case of GHG-induced ozone changes, both tropical as well as extratropical lower stratospheric ozone changes contribute to the changes in the meridional temperature gradient, while in the case of CFC-related Antarctic ozone depletion high-latitude ozone decreases in spring dominate. The quantification of the ozone-related damping of the CO₂-induced BDC strengthening might even be underestimated in our study since we do (by design) not quantify the effects of ozone changes on surface warming. It has been shown that CO₂-induced tropospheric warming might be weakened when taking ozone changes into account (Dietmüller et al. 2014; Nowack et al. 2015). Since the GHG-induced BDC strengthening is closely linked to tropical tropospheric warming (e.g., Abalos et al. 2021) leading to a stronger vertical wind shear by thermal wind balance, which alters the wave propagation and dissipation conditions (e.g., Abalos et al. 2021). Thus, weaker tropospheric warming in the tropics would further add to the damping of the BDC strengthening as long as the tropical troposphere is cooled by the CO₂-induced ozone changes. The prescribed ozone and SST fields in our uncoupled model simulations were produced by EMAC simulation with a full chemistry-climate model including ocean coupling. Thus, the 4xCO₂Ctrl simulation does not incorporate any effects of ozone changes on tropospheric warming. However, the difference to the 4xCO₂ simulation with preindustrial ozone field only quantifies the effects of ozone changes via stratospheric heating/cooling, while the contribution of ozone-induced surface temperature changes to the BDC strengthening is left for future studies to be quantified.

7. Conclusions

Our study complements a number of recent publications that aim to quantify the role of stratospheric ozone in modifying the atmospheric response to CO₂ forcing. Our main

focus is on modifications of stratospheric circulations by ozone changes, which have so far not been analyzed in detail. We find that ozone changes act as negative feedback by damping the GHG-induced BDC strengthening by about 20%. This is detected both via the residual circulation and tropical upwelling in the lower to midstratosphere (from ~100 to 5 hPa), as well as by a statistically significant reduction of the decrease in stratospheric mean AoA throughout the stratosphere. The damping of the tropical upwelling has been noted before by DallaSanta et al. (2021). Here, we further investigate the mechanism for this damping of the BDC, which is caused by reduced tropical cooling and extratropical warming in the lower stratosphere through ozone changes, acting to reduce zonal mean zonal winds via thermal wind balance. In summer, stratospheric easterlies are enhanced, attenuating vertical wave propagation, and resulting in a weaker shallow branch of the BDC. In winter, changes are generally less statistically significant and more complex, caused by weaker thermal effects of ozone due to the absence of shortwave radiation as well as by the far stronger variability in winter. While wave forcing is reduced in the lower stratosphere, contributing to the BDC damping, we find systematic increases in vertical wave propagation into the midstratosphere. Enhanced planetary wave breaking in the high latitude mid stratosphere during winter weakens the polar vortices by stronger wave–mean-flow interaction. However, the lower to midstratospheric damping of the BDC dominates changes in transport (as diagnosed via AoA) throughout the stratosphere and all seasons.

Moreover, we find that the modifications of zonal mean winds via ozone result in an earlier stratospheric final warming, thus damping the CO₂-induced prolongation of the polar vortex period by up to 50% in the SH. The shortening of the polar vortex period due to ozone changes is a result of the damping of the CO₂-induced strengthening of the polar vortices.

Overall, these findings underline the importance of the role of ozone for the circulation response to increasing CO₂ mixing ratios, indicating that ozone-circulation coupling

generally damps the atmospheric circulation response. This might have important consequences for understanding intermodel differences in the circulation response, and generally shows that a realistic representation of ozone in climate models is essential not only for its impact on chemistry, but also because it has a considerable effect on atmospheric temperatures and circulations.

Acknowledgments. This study was funded by the Helmholtz Association under Grant VH-NG-1014 Helmholtz-Hochschul-Nachwuchsforschergruppe (MACClim). This work used resources of the Deutsches Klimarechenzentrum (DKRZ) granted by its Scientific Steering Committee (WLA) under Project IDs bd1022 and id0853. RE acknowledges support by Grantová Agentura České Republiky under Grants 21-20293J and 21-03295S. PG and PJ acknowledge funding by the German Federal Ministry of Education and Research (BMBF) for the project “CMIP6-Chemie-TP1,” Grant ID FKZ 01LP1606A. Moreover, we thank Roland Walz, Michael Ponater, and Ulrike Burkhardt for their helpful suggestions and Birgit Hassler for the internal review. LH, RE, and HG designed the study. LH analyzed the data with the help by RE, HG, TB, and AK. PJ performed the simulations with support by RE and PG. LH and RE drafted the paper and all authors helped with discussions and with finalizing the manuscript.

Data availability statement. The simulation results are archived at German Climate Computing Center (DKRZ) and can be accessed at <https://zenodo.org/record/6684718>.

APPENDIX

Description of Some Submodels

This appendix contains additional material to section 2. Table A1 shows short descriptions and references of the submodels that are used for dynamics, clouds, and diagnostics.

REFERENCES

- Abalos, M., L. Polvani, N. Calvo, D. Kinnison, F. Ploeger, W. Randel, and S. Solomon, 2019: New insights on the impact of ozone-depleting substances on the Brewer–Dobson circulation. *J. Geophys. Res. Atmos.*, **124**, 2435–2451, <https://doi.org/10.1029/2018JD029301>.
- , and Coauthors, 2021: The Brewer–Dobson circulation in CMIP6. *Atmos. Chem. Phys.*, **21**, 13 571–13 591, <https://doi.org/10.5194/acp-21-13571-2021>.
- Andrews, D. G., J. R. Holton, and C. B. Leovy, 1987: *Middle Atmosphere Dynamics*. Academic Press, 489 pp.
- Ayarzagüena, B., and Coauthors, 2020: Uncertainty in the response of sudden stratospheric warmings and stratosphere–troposphere coupling to quadrupled CO₂ concentrations in CMIP6 models. *J. Geophys. Res. Atmos.*, **125**, e2019JD032345, <https://doi.org/10.1029/2019JD032345>.
- Baldwin, M. P., and Coauthors, 2021: Sudden stratospheric warmings. *Rev. Geophys.*, **59**, e2020RG000708, <https://doi.org/10.1029/2020RG000708>.
- Baumgaertner, A. J. G., P. Jöckel, A. D. Aylward, and M. J. Harris, 2013: Simulation of particle precipitation effects on the atmosphere with the MESSy model system. *Climate and Weather of the Sun–Earth System (CAWSES)*, F. J. Lübken, Ed., Springer, 301–316, https://doi.org/10.1007/978-94-007-4348-9_17.
- Birner, T., and E. J. Charlesworth, 2017: On the relative importance of radiative and dynamical heating for tropical tropopause temperatures. *J. Geophys. Res. Atmos.*, **122**, 6782–6797, <https://doi.org/10.1002/2016JD026445>.
- Brewer, A. W., 1949: Evidence for a world circulation provided by the measurements of helium and water vapour distribution in the stratosphere. *Quart. J. Roy. Meteor. Soc.*, **75**, 351–363, <https://doi.org/10.1002/qj.49707532603>.
- Butchart, N., and A. A. Scaife, 2001: Removal of chlorofluorocarbons by increased mass exchange between the stratosphere and troposphere in a changing climate. *Nature*, **410**, 799–802, <https://doi.org/10.1038/35071047>.
- , and Coauthors, 2010: Chemistry–climate model simulations of twenty-first century stratospheric climate and circulation changes. *J. Climate*, **23**, 5349–5374, <https://doi.org/10.1175/2010JCLI3404.1>.
- Byrne, N. J., and T. G. Shepherd, 2018: Seasonal persistence of circulation anomalies in the Southern Hemisphere stratosphere and its implications for the troposphere. *J. Climate*, **31**, 3467–3483, <https://doi.org/10.1175/JCLI-D-17-0557.1>.
- , —, T. Woolings, and R. A. Plumb, 2017: Nonstationarity in Southern Hemisphere climate variability associated with the seasonal breakdown of the stratospheric polar vortex. *J. Climate*, **30**, 7125–7139, <https://doi.org/10.1175/JCLI-D-17-0097.1>.
- Ceppi, P., and T. G. Shepherd, 2019: The role of the stratospheric polar vortex for the austral jet response to greenhouse gas forcing. *Geophys. Res. Lett.*, **46**, 6972–6979, <https://doi.org/10.1029/2019GL082883>.
- Charlesworth, E. J., T. Birner, and J. R. Albers, 2019: Ozone transport–radiation feedbacks in the tropical tropopause layer. *Geophys. Res. Lett.*, **46**, 14 195–14 202, <https://doi.org/10.1029/2019GL084679>.
- Charlton, A. J., and L. M. Polvani, 2007: A new look at stratospheric sudden warmings. Part I: Climatology and modeling benchmarks. *J. Climate*, **20**, 449–469, <https://doi.org/10.1175/JCLI3996.1>.
- Chiodo, G., and L. M. Polvani, 2017: Reduced Southern Hemispheric circulation response to quadrupled CO₂ due to stratospheric ozone feedback. *Geophys. Res. Lett.*, **44**, 465–474, <https://doi.org/10.1002/2016GL071011>.
- , and —, 2019: The response of the ozone layer to quadrupled CO₂ concentrations: Implications for climate. *J. Climate*, **32**, 7629–7642, <https://doi.org/10.1175/JCLI-D-19-0086.1>.
- , —, D. R. Marsh, A. Stenke, W. Ball, E. Rozanov, S. Muthers, and K. Tsigaridis, 2018: The response of the ozone layer to quadrupled CO₂ concentrations. *J. Climate*, **31**, 3893–3907, <https://doi.org/10.1175/JCLI-D-17-0492.1>.
- Chrysanthou, A., A. C. Maycock, and M. P. Chipperfield, 2020: Decomposing the response of the stratospheric Brewer–Dobson circulation to an abrupt quadrupling in CO₂. *Wea. Climate Dyn.*, **1**, 155–174, <https://doi.org/10.5194/wcd-1-155-2020>.
- Dacie, S., and Coauthors, 2019: A 1D RCE study of factors affecting the tropical tropopause layer and surface climate. *J. Climate*, **32**, 6769–6782, <https://doi.org/10.1175/JCLI-D-18-0778.1>.
- DallaSanta, K., C. Orbe, D. Rind, L. Nazarenko, and J. Jonas, 2021: Dynamical and trace gas responses of the quasi-biennial

- oscillation to increased CO₂. *J. Geophys. Res. Atmos.*, **126**, e2020JD034151, <https://doi.org/10.1029/2020JD034151>.
- Dietmüller, S., M. Ponater, and R. Sausen, 2014: Interactive ozone induces a negative feedback in CO₂-driven climate change simulations. *J. Geophys. Res. Atmos.*, **119**, 1796–1805, <https://doi.org/10.1002/2013JD020575>.
- , and Coauthors, 2016: A new radiation infrastructure for the Modular Earth Submodel System (MESSy, based on version 2.51). *Geosci. Model Dev.*, **9**, 2209–2222, <https://doi.org/10.5194/gmd-9-2209-2016>.
- , H. Garny, F. Plöger, P. Jöckel, and D. Cai, 2017: Effects of mixing on resolved and unresolved scales on stratospheric age of air. *Atmos. Chem. Phys.*, **17**, 7703–7719, <https://doi.org/10.5194/acp-17-7703-2017>.
- , and Coauthors, 2018: Quantifying the effect of mixing on the mean age of air in CCMVal-2 and CCM1 models. *Atmos. Chem. Phys.*, **18**, 6699–6720, <https://doi.org/10.5194/acp-18-6699-2018>.
- Dobson, G. M. B., 1956: Origin and distribution of the polyatomic molecules in the atmosphere. *Proc. Roy. Soc.*, **236A**, 187–193, <https://doi.org/10.1098/rspa.1956.0127>.
- Edmon, H. J., B. J. Hoskins, and M. E. McIntyre, 1980: Eliassen–Palm cross sections for the troposphere. *J. Atmos. Sci.*, **37**, 2600–2616, [https://doi.org/10.1175/1520-0469\(1980\)037<2600:EPCSFT>2.0.CO;2](https://doi.org/10.1175/1520-0469(1980)037<2600:EPCSFT>2.0.CO;2).
- Eichinger, R., and P. Sacha, 2020: Overestimated acceleration of the advective Brewer–Dobson circulation due to stratospheric cooling. *Quart. J. Roy. Meteor. Soc.*, **146**, 3850–3864, <https://doi.org/10.1002/qj.3876>.
- , P. Jöckel, S. Brinkop, M. Werner, and S. Lossow, 2015: Simulation of the isotopic composition of stratospheric water vapour—Part 1: Description and evaluation of the EMAC model. *Atmos. Chem. Phys.*, **15**, 5537–5555, <https://doi.org/10.5194/acp-15-5537-2015>.
- , and Coauthors, 2019: The influence of mixing on the stratospheric age of air changes in the 21st century. *Atmos. Chem. Phys.*, **19**, 921–940, <https://doi.org/10.5194/acp-19-921-2019>.
- , H. Garny, P. Šácha, J. Danker, S. Dietmüller, and S. Oberländer-Hayn, 2020: Effects of missing gravity waves on stratospheric dynamics; Part 1: Climatology. *Climate Dyn.*, **54**, 3165–3183, <https://doi.org/10.1007/s00382-020-05166-w>.
- Eyring, V., S. Bony, G. A. Meehl, C. A. Senior, B. Stevens, R. J. Stouffer, and K. E. Taylor, 2016: Overview of the Coupled Model Intercomparison Project phase 6 (CMIP6) experimental design and organization. *Geosci. Model Dev.*, **9**, 1937–1958, <https://doi.org/10.5194/gmd-9-1937-2016>.
- Frank, F., P. Jöckel, S. Gromov, and M. Dameris, 2018: Investigating the yield of H₂O and H₂ from methane oxidation in the stratosphere. *Atmos. Chem. Phys.*, **18**, 9955–9973, <https://doi.org/10.5194/acp-18-9955-2018>.
- Garcia, R. R., and W. J. Randel, 2008: Acceleration of the Brewer–Dobson circulation due to increases in greenhouse gases. *J. Atmos. Sci.*, **65**, 2731–2739, <https://doi.org/10.1175/2008JAS2712.1>.
- Garny, H., T. Birner, H. Bönisch, and F. Bunzel, 2014: The effects of mixing on age of air. *J. Geophys. Res. Atmos.*, **119**, 7015–7034, <https://doi.org/10.1002/2013JD021417>.
- Giorgetta, M. A., and L. Bengtsson, 1999: Potential role of the quasi-biennial oscillation in the stratosphere-troposphere exchange as found in water vapour in general circulation model experiments. *J. Geophys. Res.*, **104**, 6003–6019, <https://doi.org/10.1029/1998JD200112>.
- Haigh, J. D., and J. A. Pyle, 1982: Ozone perturbation experiments in a two-dimensional circulation model. *Quart. J. Roy. Meteor. Soc.*, **108**, 551–574, <https://doi.org/10.1002/qj.49710845705>.
- Hall, T. M., and R. A. Plumb, 1994: Age as a diagnostic of stratospheric transport. *J. Geophys. Res.*, **99**, 1059–1070, <https://doi.org/10.1029/93JD03192>.
- Haynes, P. H., M. E. McIntyre, T. G. Shepherd, C. J. Marks, and K. P. Shine, 1991: On the “downward control” of extratropical diabatic circulations by eddy-induced mean zonal forces. *J. Atmos. Sci.*, **48**, 651–678, [https://doi.org/10.1175/1520-0469\(1991\)048<0651:OTCOED>2.0.CO;2](https://doi.org/10.1175/1520-0469(1991)048<0651:OTCOED>2.0.CO;2).
- IPCC, 2018: *Global Warming of 1.5°C*. Cambridge University Press, 616 pp., <https://doi.org/10.1017/9781009157940>.
- Ivanciu, I., K. Matthes, A. Biastoch, S. Wahl, and J. Harlaß, 2022: Twenty-first century Southern Hemisphere impacts of ozone recovery and climate change from the stratosphere to the ocean. *Wea. Climate Dyn.*, **3**, 139–171, <https://doi.org/10.5194/wcd-3-139-2022>.
- Jöckel, P., R. Sander, A. Kerkweg, H. Tost, and J. Lelieveld, 2005: Technical note: The Modular Earth Submodel System (MESSy)—A new approach towards Earth system modeling. *Atmos. Chem. Phys.*, **5**, 433–444, <https://doi.org/10.5194/acp-5-433-2005>.
- , and Coauthors, 2006: The atmospheric chemistry general circulation model ECHAM5/MESSy1: Consistent simulation of ozone from the surface to the mesosphere. *Atmos. Chem. Phys.*, **6**, 5067–5104, <https://doi.org/10.5194/acp-6-5067-2006>.
- , A. Kerkweg, J. Buchholz-Dietsch, H. Tost, R. Sander, and A. Pozzer, 2008: Technical note: Coupling of chemical processes with the Modular Earth Submodel System (MESSy) submodel TRACER. *Atmos. Chem. Phys.*, **8**, 1677–1687, <https://doi.org/10.5194/acp-8-1677-2008>.
- , and Coauthors, 2010: Development cycle 2 of the Modular Earth Submodel System (MESSy2). *Geosci. Model Dev.*, **3**, 717–752, <https://doi.org/10.5194/gmd-3-717-2010>.
- , and Coauthors, 2016: Earth system chemistry integrated modelling (ESCI-MO) with the modular earth submodel system (MESSy, version 2.51). *Geosci. Model Dev.*, **9**, 1153–1200, <https://doi.org/10.5194/gmd-9-1153-2016>.
- Jucker, M., 2021: Scaling of Eliassen–Palm flux vectors. *Atmos. Sci. Lett.*, **22**, e1020, <https://doi.org/10.1002/asl.1020>.
- Karpechko, A. Y., and Coauthors, 2022: Northern Hemisphere stratosphere-troposphere circulation change in CMIP6 models: 1. Inter-model spread and scenario sensitivity. *J. Geophys. Res. Atmos.*, **127**, e2022JD036992, <https://doi.org/10.1029/2022JD036992>.
- Kerkweg, A., R. Sander, H. Tost, and P. Jöckel, 2006: Technical note: Implementation of prescribed (OFFLEM), calculated (ONLEM), and pseudo-emissions (TNUDGE) of chemical species in the modular earth submodel system (MESSy). *Atmos. Chem. Phys.*, **6**, 3603–3609, <https://doi.org/10.5194/acp-6-3603-2006>.
- le Texier, H., S. Solomon, and R. R. Garcia, 1988: The role of molecular hydrogen and methane oxidation in the water vapour budget of the stratosphere. *Quart. J. Roy. Meteor. Soc.*, **114**, 281–295, <https://doi.org/10.1002/qj.49711448002>.
- Li, F., J. Austin, and J. Wilson, 2008: The strength of the Brewer–Dobson circulation in a changing climate: Coupled chemistry–climate model simulations. *J. Climate*, **21**, 40–57, <https://doi.org/10.1175/2007JCLI1663.1>.
- Marsh, D. R., J.-F. Lamarque, A. J. Conley, and L. M. Polvani, 2016: Stratospheric ozone chemistry feedbacks are not critical for the determination of climate sensitivity in CESM1(WACCM).

- Geophys. Res. Lett.*, **43**, 3928–3934, <https://doi.org/10.1002/2016GL068344>.
- Maycock, A. C., M. M. Joshi, K. P. Shine, and A. A. Scaife, 2013: The circulation response to idealized changes in stratospheric water vapor. *J. Climate*, **26**, 545–561, <https://doi.org/10.1175/JCLI-D-12-00155.1>.
- , —, —, S. M. Davis, and K. H. Rosenlof, 2014: The potential impact of changes in lower stratospheric water vapour on stratospheric temperatures over the past 30 years. *Quart. J. Roy. Meteor. Soc.*, **140**, 2176–2185, <https://doi.org/10.1002/qj.2287>.
- McLandress, C., and T. G. Shepherd, 2009: Simulated anthropogenic changes in the Brewer–Dobson circulation, including its extension to high latitudes. *J. Climate*, **22**, 1516–1540, <https://doi.org/10.1175/2008JCLI2679.1>.
- Mindlin, J., T. G. Shepherd, C. Vera, and M. Osman, 2021: Combined effects of global warming and ozone depletion/recovery on Southern Hemisphere atmospheric circulation and regional precipitation. *Geophys. Res. Lett.*, **48**, e2021GL092568, <https://doi.org/10.1029/2021GL092568>.
- Muthers, S., and Coauthors, 2014: The coupled atmosphere–chemistry–ocean model SOCOL-MPIOM. *Geosci. Model Dev.*, **7**, 2157–2179, <https://doi.org/10.5194/gmd-7-2157-2014>.
- Nissen, K. M., K. Matthes, U. Langematz, and B. Mayer, 2007: Towards a better representation of the solar cycle in general circulation models. *Atmos. Chem. Phys.*, **7**, 5391–5400, <https://doi.org/10.5194/acp-7-5391-2007>.
- Nowack, P. J., N. L. Abraham, A. C. Maycock, P. Braesicke, J. M. Gregory, M. M. Joshi, A. Osprey, and J. A. Pyle, 2015: A large ozone-circulation feedback and its implications for global warming assessments. *Nat. Climate Change*, **5**, 41–45, <https://doi.org/10.1038/nclimate2451>.
- , —, P. Braesicke, and J. A. Pyle, 2018: The impact of stratospheric ozone feedbacks on climate sensitivity estimates. *J. Geophys. Res. Atmos.*, **123**, 4630–4641, <https://doi.org/10.1002/2017JD027943>.
- Oberländer-Hayn, S., and Coauthors, 2016: Is the Brewer–Dobson circulation increasing or moving upward? *Geophys. Res. Lett.*, **43**, 1772–1779, <https://doi.org/10.1002/2015GL067545>.
- Okamoto, K., K. Sato, and H. Akiyoshi, 2011: A study on the formation and trend of the Brewer–Dobson circulation. *J. Geophys. Res.*, **116**, D10117, <https://doi.org/10.1029/2010JD014953>.
- Pisof, P., and Coauthors, 2021: Stratospheric contraction caused by increasing greenhouse gases. *Environ. Res. Lett.*, **16**, 064038, <https://doi.org/10.1088/1748-9326/abfe2b>.
- Roeckner, E., and Coauthors, 2006: Sensitivity of simulated climate to horizontal and vertical resolution in the ECHAM5 atmosphere model. *J. Climate*, **19**, 3771–3791, <https://doi.org/10.1175/JCLI3824.1>.
- Shepherd, T. G., and C. McLandress, 2011: A robust mechanism for strengthening of the Brewer–Dobson circulation in response to climate change: Critical-layer control of subtropical wave breaking. *J. Atmos. Sci.*, **68**, 784–797, <https://doi.org/10.1175/2010JAS3608.1>.
- Stocker, T. F., and Coauthors, 2013: *Climate Change 2013: The Physical Science Basis*. Cambridge University Press, 1535 pp., <https://doi.org/10.1017/CBO9781107415324>.
- Szopa, S., and Coauthors, 2021: Short-lived climate forcings. *Climate Change 2021: The Physical Science Basis*, V. Masson-Delmotte et al., Eds., Cambridge University Press, 817–922.
- Thompson, D. W. J., S. Solomon, P. J. Kushner, M. H. England, K. M. Grise, and D. J. Karoly, 2011: Signatures of the Antarctic ozone hole in Southern Hemisphere surface climate change. *Nat. Geosci.*, **4**, 741–749, <https://doi.org/10.1038/ngeo1296>.
- Tost, H., 2006: Global modelling of cloud, convection and precipitation: Influences on trace gases and aerosols. Ph.D. thesis, University of Bonn, 198 pp., <https://hdl.handle.net/20.500.11811/2602>.
- , P. Jöckel, and J. Lelieveld, 2006: Influence of different convection parameterisations in a GCM. *Atmos. Chem. Phys.*, **6**, 5475–5493, <https://doi.org/10.5194/acp-6-5475-2006>.
- Vallis, G. K., P. Zurita-Gotor, C. Cairns, and J. Kidston, 2015: Response of the large-scale structure of the atmosphere to global warming. *Quart. J. Roy. Meteor. Soc.*, **141**, 1479–1501, <https://doi.org/10.1002/qj.2456>.
- Waugh, D., and T. Hall, 2002: Age of stratospheric air: Theory, observations and models. *Rev. Geophys.*, **40**, 1010, <https://doi.org/10.1029/2000RG000101>.
- Winterstein, F., and P. Jöckel, 2021: Methane chemistry in a nutshell—The new submodels CH4 (v1.0) and TRSYNC (v1.0) in MESSy (v2.54.0). *Geosci. Model Dev.*, **14**, 661–674, <https://doi.org/10.5194/gmd-14-661-2021>.
- Yoon, S., D. W. J. Thompson, S. Solomon, and S.-Y. Kim, 2020: The key role of coupled chemistry–climate interactions in Tropical stratospheric temperature variability. *J. Climate*, **33**, 7619–7629, <https://doi.org/10.1175/JCLI-D-20-0071.1>.